

Few-Shot Demonstration-Driven Task Coordination and Trajectory Execution for Multi-Robot Systems

Taehyeon Kim^{1†}, Vishnunandan L.N. Venkatesh^{1†}, and Byung-Cheol Min²

Abstract—In this paper, we propose a novel few-shot learning framework for multi-robot systems that integrate both spatial and temporal elements: Few-Shot Demonstration-Driven Task Coordination and Trajectory Execution (DDACE). Our approach leverages temporal graph networks for learning task-agnostic temporal sequencing and Gaussian Processes for spatial trajectory modeling, ensuring modularity and generalization across various tasks. By decoupling temporal and spatial aspects, DDACE requires only a small number of demonstrations, significantly reducing data requirements compared to traditional learning from demonstration approaches. To validate our proposed framework, we conducted extensive experiments in task environments designed to assess various aspects of multi-robot coordination—such as multi-sequence execution, multi-action dynamics, complex trajectory generation, and heterogeneous configurations. The experimental results demonstrate that our approach successfully achieves task execution under few-shot learning conditions and generalizes effectively across dynamic and diverse settings. This work underscores the potential of modular architectures in enhancing the practicality and scalability of multi-robot systems in real-world applications. Additional materials are available at <https://sites.google.com/view/ddace>.

I. INTRODUCTION

LEARNING from Demonstration (LfD) has emerged as a transformative paradigm in robotics, enabling systems to acquire complex behaviors efficiently by leveraging human-provided demonstrations. Bypassing the need for explicitly programmed rules and reward engineering, LfD allows robots to generalize skills from demonstrations, significantly lowering the barrier to the deployment of intelligent systems in various domains [1], [2]. The applicability of LfD spans a wide range of fields, from industrial automation to service robotics, where human expertise can be intuitively transferred to robotic agents [3].

Although effective in single-agent settings, applying LfD to Multi-Robot Systems (MRS) introduces unique challenges. Multi-robot tasks often involve intricate spatial-temporal interdependencies [4], requiring synchronized behaviors across heterogeneous agents with diverse capabilities [5], [6]. This is critical in sequential task execution (e.g., sports, collaborative assembly) and heterogeneous team coordination (e.g., logistics, disaster response), where learning temporal action sequences - rather than only final goal states - is essential for robust coordination.

However, most LfD methods are data-hungry, task-specific, and overlook modeling of spatial and temporal aspects, lim-

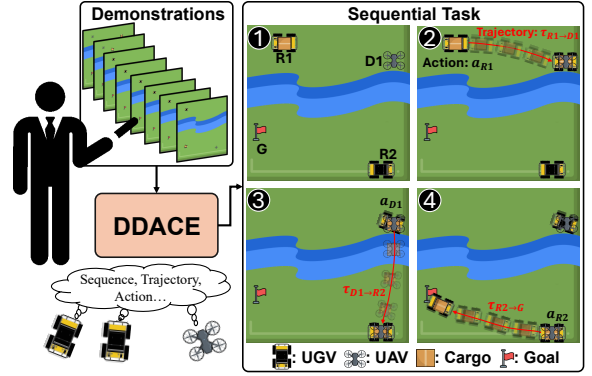


Fig. 1: Concept for few-shot Demonstration-Driven Task Coordination and Trajectory Execution for multi-robot systems (DDACE). A human expert demonstrates task, from which the robots learn both sequences, composed of multiple actions and trajectories. a refers to high-level actions taken by the robot, and τ is the corresponding trajectory from start \rightarrow goal.

iting generalization in few-shot settings [2], [7]. Many focus solely on achieving goal states, neglecting action sequencing, which is vital in applications demanding trajectory fidelity. Although some domain-specific work, such as robot soccer [8], [9], considers sequential behaviors, it usually relies on specialized reward functions, constraining adaptability. Consequently, there remains a critical need for an LfD framework that not only operates efficiently under few-shot constraints but also generalizes across multi-robot tasks while explicitly modeling the temporal dependencies crucial for effective coordination.

This work addresses these limitations through a dual stage, decoupled framework—DDACE—which separately learns temporal sequences via a Temporal Graph Network (TGN) and spatial trajectories via Gaussian Processes (GP). Demonstrations are represented as graphs of robots, goals, and interactive objects, and spectral clustering is applied to extract key interdependencies for the TGN. The TGN employs Graph Attention Networks (GATs) and Gated Recurrent Units (GRUs) to capture temporal dynamics, while the GP module generates adaptable trajectories between start and goal points, applying normalization to enhance generalizability [10]. The proposed approach is evaluated on a diverse set of categorized tasks, each designed to assess different aspects of multi-robot sequential operations. This modular design enables minimal-data learning for coordinated action sequencing and robust trajectory generalization across varied multi-robot tasks.

The key contributions of this work are summarized as follows:

- **DDACE** is proposed as a novel few-shot Learning from Demonstration framework for multi-robot systems that explicitly decouples temporal and spatial learning. Task-agnostic action sequences are learned using a TGN, and con-

[†] Equal Contribution

¹Purdue University, West Lafayette, IN, USA. [kim4435, lvenkate]@purdue.edu.

²Indiana University Bloomington, Bloomington, IN, USA. minb@iu.edu.

tinuous spatial trajectories are modeled using GP, enabling modularity and generalization across diverse coordination scenarios.

- A TGN architecture augmented with spectral clustering for graph construction is designed to learn inter-robot connections and temporal dependencies from only a handful of demonstrations, facilitating robust, task-agnostic multi-action sequence prediction in few-shot settings.
- DDACE is validated on diverse tasks involving heterogeneous agents, multi-sequence coordination, and complex trajectories. Beyond benchmarking under few-shot constraints and demonstrating real-world transfer, case studies on team size and action space complexity are conducted to analyze scalability and adaptability in practical MRS deployments.

II. RELATED WORKS

Learning from demonstration (LfD) enables multi-robot systems to acquire complex behaviors through intuitive, human-led instruction. Methods include teleoperation-based learning for navigation and manipulation [11], [12], reinforcement learning with state-space automata for robot soccer [9], [13], and adaptive confidence-based mechanisms for interactive demonstrations [14]. Others use geometric CAD models for structured collaboration [6] or vision-based demonstrations with probabilistic models such as Gaussian Mixture Models for bi-manual tasks [15]. These approaches often face challenges of task specificity, reliance on large datasets, and limited intuitive, vision-based communication [1], [2], [16]. More recent frameworks integrate interaction keypoints and reinforcement learning for coordination [17], but do not explicitly address spatiotemporal modeling.

Graph Neural Networks (GNNs) naturally represent multi-robot systems (MRS) as graphs, with robots as nodes and interactions as edges [18], capturing relational dependencies essential for coordination [19]. Applications include decentralized path planning for collision-free navigation in partially observable environments [19], [20] and real-world deployments via ROS2 [18]. In task allocation, GNNs solve combinatorial problems such as the Linear Sum Assignment Problem (LSAP) using heterogeneous graphs [21], [22], sometimes enhanced with heuristics like the Consensus-Based Bundle Algorithm (CBBA) [23]. They also enable cooperative behaviors—flocking, coverage, and formation control [18], [23]–[26]. Hierarchical variants like H2GNN further improve exploration efficiency by aggregating spatial information [24].

Recent state-of-the-art end-to-end multi-agent learning approaches, such as MADiff [27] and MADT [28], demonstrate strong coordination in offline MARL domains. MADiff uses diffusion models to jointly generate multi-agent action or trajectory sequences, while MADT applies transformer-based sequence modeling for decision making. Both approaches rely on large offline datasets, which is incompatible with few shot demonstration learning, and integrate temporal and spatial learning within a single model, limiting modularity and adaptability. They also omit progress parameterized geometry for flexible start and goal adaptation—capabilities critical for few shot multi-robot learning.

In contrast, DDACE employs a hierarchically decoupled framework that learns temporal action sequencing and spatial motion generation independently. It generalizes from minimal demonstrations by extracting essential robot–object interactions without large datasets or handcrafted rewards, unlike GNN-based or end-to-end MRS approaches, it leverages graph-based temporal reasoning and progress-parameterized geometry for rapid, few-shot adaptation to diverse multi-robot coordination tasks.

III. METHODOLOGY

A. Problem Definition

Let $D = \{d_1, d_2, \dots, d_k\}$ be a set of demonstrations for coordinated multi-robot tasks. Each demonstration d_i is represented by a *demonstration graph* $G_i = (N_i, E_i)$, where:

- N_i represents robots, goals, and other interactive objects.
- E_i encodes *interdependencies* such as enabling relations (finish→start) or physical interaction constraints.

Each d_i contains two data modalities, reflecting the structure of a hierarchical policy:

- Temporal sequences $\mathbf{S}_i^{\text{demo}}$: ordered action tokens specifying *when* each robot-specific operation occurs, capturing high-level task logic and partial-order constraints without prescribing motion geometry.
- Spatial trajectories $\mathbf{T}_i^{\text{demo}}$: continuous paths from x_0 to x_T , reparameterized by progress $s \in [0, 1]$ so that geometry is modeled independently of absolute time.

The *spatial* modality is a geometry-only path $\mathbf{x}(s)$, $s \in [0, 1]$, and the *temporal* modality is a partial order $\langle \mathcal{A}, \prec \rangle$ over action tokens, with \prec from inferred enabling edges; only ordering is modeled, not durations.

Demonstrations are assumed to be optimal and not noisy, encoding coherent multi-step task sequences that can be used to infer both temporal partial orders and spatial trajectories. This assumption ensures that meaningful patterns can be extracted from limited data in few-shot learning settings.

The learning objective is defined as: $F : D \rightarrow (\mathbf{S}, \mathbf{T})$, where \mathbf{S} constitutes the *high-level policy* (temporal coordination) and \mathbf{T} constitutes the *low-level policy* (spatial motion generation), with temporal reasoning explicitly decoupled from spatial processing.

1) Sequence Learning via Temporal Graph Networks:

$$f_T(C(G_i); \theta) \approx \mathbf{S}_i^{\text{demo}} \quad (1)$$

Here $C(G_i)$ denotes a spectral clustering of G_i to extract key inter-node relations. A Temporal Graph Network (TGN), parameterized by θ , is used to learn the temporal ordering such that predicted sequences match those in the demonstrations.

2) Trajectory Learning via Gaussian Processes:

$$f_S(x_0, x_T; \phi) \approx \mathbf{T}_i^{\text{demo}} \quad (2)$$

Here ϕ denotes the Gaussian Process hyperparameters. With z-transform scaling in a canonical coordinate frame, f_S reproduces demonstrated paths and synthesizes novel, geometrically consistent trajectories without committing to specific execution timing.

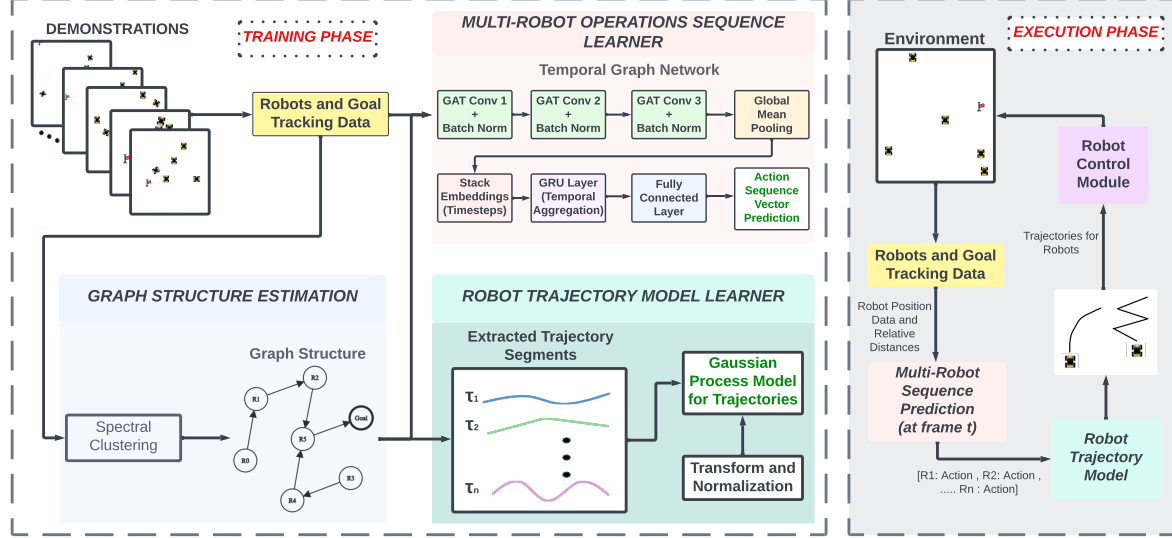


Fig. 2: Overview of the proposed DDACE framework. In the training phase, demonstration data is preprocessed, graph structures are extracted via spectral clustering, and the Temporal Graph Networks (TGN) and Gaussian Processes (GP) models are trained independently. During the execution phase, the trained models predict coordinated action sequences and generate spatial trajectories for new scenarios, enabling adaptive and efficient multi-robot task execution.

3) *Execution Semantics*: At decision epochs (periodic or event-triggered), the high-level policy f_T selects the next action consistent with the learned partial order. For motion tokens $a \in \mathcal{A}$, the low-level policy f_S outputs a progress-parameterized path $\mathbf{x}_a(s)$, tracked by a controller. This separation ensures temporal logic governs *when* actions occur and spatial processing governs *how* motion is executed, avoiding ambiguity between geometry and timestamps.

The objective is to learn f_T and f_S such that their outputs jointly reproduce and generalize $\mathbf{S}_i^{\text{demo}}$ and $\mathbf{T}_i^{\text{demo}}$ for few-shot coordinated multi-robot tasks.

B. Temporal Graph Networks (TGNs)

1) *Preprocessing*: Let $d_i \in D$ be a multi-robot task demonstration recorded as a CSV, where each row corresponds to a discrete time step $t \in 1, \dots, T_i$ and contains node features and labels. Node features are the (x, y) coordinates of each entity in N_i (e.g., robots, goals, objects), while labels indicate their action state or activity. From each d_i , node features are reshaped into $\mathbf{X}_i \in \mathbb{R}^{T_i \times |N_i| \times 2}$ and labels into $\mathbf{L}_i \in \mathbb{R}^{T_i \times |N_i|}$, capturing spatial positions and dynamic state changes over time.

A critical component of our preprocessing is the automatic segmentation of demonstrations into high-level action steps. This is achieved by selecting keyframes from \mathbf{L}_i where a nonzero activity label appears and differs from the previous frame:

$$\mathbf{L}_i(t) \neq \mathbf{0} \quad \text{and} \quad \mathbf{L}_i(t) \neq \mathbf{L}_i(t-1). \quad (3)$$

This rule infers substep boundaries directly from observed state changes, ensuring they are fully derived from demonstration data without reliance on manually pre-segmented inputs.

The final output is a sequence of graph snapshots containing node features and labels, condensed to key events to reduce redundancy and focus learning on critical transitions for robust multi-robot coordination and manipulation.

2) *Spectral Clustering*: From the keyframe sequence of d_i , we extract a set of directed edges E_i , and aggregate them across all demonstrations into the unique edge set $\mathcal{E} = \{e_1, \dots, e_m\}$. The frequency of each edge is

$$F(e) = \sum_{i=1}^k f_e(d_i), \quad (4)$$

where $f_e(d_i)$ counts occurrences of e in d_i .

We construct a weighted adjacency matrix $\mathbf{A} \in \mathbb{R}^{m \times m}$ with diagonal entries $A_{jj} = F(e_j)$ and zeros elsewhere. The degree matrix \mathbf{D} has $D_{jj} = \sum_l A_{jl}$. The unnormalized graph Laplacian is then $\mathbf{L} = \mathbf{D} - \mathbf{A}$.

Solving the eigenproblem $\mathbf{L}\mathbf{v} = \lambda\mathbf{v}$, we use eigenvectors associated with the smallest non-zero eigenvalues to cluster edges into K groups. This yields the refined edge set

$$E' = \{e \in \mathcal{E} \mid \mathcal{C}(e) \text{ is assigned}\}, \quad (5)$$

with index E' guiding node aggregation in the TGN's spatial encoder.

This process filters raw connectivity to retain only the most persistent inter-node relationships observed across demonstrations. By embedding these refined structural priors, the temporal model gains robustness and better generalization in few-shot multi-robot coordination.

3) *Graph Attention Networks and Gated Recurrent Units*: Our model is designed to effectively learn spatiotemporal information by decoupling spatial and temporal encoding. In multi-robot tasks, the spatial interactions among robots and objects and their temporal evolution are inherently distinct. The spatial encoding phase captures the relational configuration at each keyframe, providing essential context for subsequent sequence learning, while the temporal encoding phase models the evolution of these configurations over time.

Let $\mathbf{X}_i^{(t)} \in \mathbb{R}^{|N_i| \times 2}$ denote the node feature matrix at keyframe t of demonstration $d_i \in D$, where the rows correspond to entities in the node set N_i . In the spatial encoding stage, these features are processed through a series of GATs.

Importantly, the connectivity structure, represented by the refined edge index \mathbf{E}' , is derived from the spectral clustering procedure described above.

We initialize the node embeddings at keyframe t as $h_i^{(0)} = \mathbf{X}_i^{(t)}$. The embeddings are then updated over $L = 3$ GAT layers as follows:

$$h_i^{(l)} = \sigma \left(\text{Dropout} \left(\text{BN} \left(\text{GAT}^{(l)} \left(h_i^{(l-1)}, \mathbf{E}' \right) \right) \right) \right), \quad l = 1, 2, 3, \quad (6)$$

where $\text{GAT}^{(l)}(\cdot)$ denotes the l^{th} GAT layer employing a multi-head attention mechanism with two heads per layer, $\text{BN}(\cdot)$ is Batch Normalization, $\sigma(\cdot)$ represents the ReLU activation function, and Dropout is applied for regularization. A global pooling operation, $\text{Pool}(\cdot)$, aggregates the final node embeddings $h_i^{(3)}$ into a graph-level embedding:

$$g_i^{(t)} = \text{Pool} \left(h_i^{(3)} \right). \quad (7)$$

The sequence of graph-level embeddings $\{g_i^{(t)}\}_{t \in \mathcal{K}_i}$, where \mathcal{K}_i is the set of keyframe indices for demonstration d_i , serves as input to the temporal encoding stage. This stage employs a two-layer GRU in an autoregressive fashion. Specifically, at each time step t , the GRU takes the current graph-level embedding $g_i^{(t)}$ along with the previous hidden state $s_i^{(t-1)}$ (initialized as $s_i^{(0)} = \mathbf{0}$) to produce an updated hidden state:

$$s_i^{(t)} = \text{GRU} \left(g_i^{(t)}, s_i^{(t-1)} \right). \quad (8)$$

This autoregressive structure enables the GRU to predict the next state based on the accumulated historical context. The output at each time step, $s_i^{(t)}$, is then passed through a fully connected layer $f_{\text{FC}}(\cdot)$ to yield the predicted action for that time step:

$$\hat{s}_i^{(t)} = f_{\text{FC}} \left(s_i^{(t)} \right). \quad (9)$$

By recursively updating the hidden state and predicting the subsequent output, our TGN generates the action sequence one step at a time.

By integrating refined spatial encoding via three GAT layers—with edge connectivity informed by spectral clustering—and autoregressive temporal modeling via GRUs, our model robustly captures both inter-node relationships and their evolution over time. This approach is particularly effective in few-shot learning scenarios, enhancing the model’s generalization across diverse multi-robot tasks.

C. Gaussian Processes

Each demonstration dataset D_k consists of positional coordinates for N robots and goal node at discrete timesteps, expressed as:

$$D_k = \{\mathbf{x}_i^{(t)} \mid \mathbf{x}_i^{(t)} \in \mathbb{R}^2, i \in \{1, \dots, N, N+1\}, t = 1, \dots, T_k\}, \quad (10)$$

where i indexes the robots ($1, \dots, N$) and the goal node ($N+1$), and T_k denotes the total number of frames in demonstration k .

Following preprocessing, complete trajectory segments were extracted from the generated temporal graph sequences. A trajectory segment $\tau_{s \rightarrow t}^{(k)}$, corresponding to the movement of

a robot from a source node s to a target node t within demonstration k , is defined as:

$$\tau_{s \rightarrow t}^{(k)} = \{\mathbf{x}_s^{(m)} \mid m = t_{\text{start}}, \dots, t_{\text{end}}\}, \quad (11)$$

where t_{start} and t_{end} represent the frame indices marking the beginning and end of a continuous robot movement segment. Each trajectory segment was annotated with its corresponding demonstration index, source-target identifiers, and temporal boundaries. This structured annotation provided a consistent dataset of trajectory segments for subsequent trajectory modeling.

To generalize demonstrations for novel contexts, GP regression encoded motion primitives for each unique source-target robot pair. Before training, trajectories were normalized, aligned to a canonical frame, and uniformly resampled into fixed-length 100-point sequences for consistency. For each aligned source-target trajectory set, two GP models (x_{GP} and y_{GP}) were trained to map normalized time to x and y positions, using an RBF + WhiteKernel to capture spatial correlations and noise, with training data aggregated from all resampled segments for that pair.

D. Execution Phase

At runtime, the DDACE framework operates hierarchically, with the TGN serving as the high-level policy and the GP-based motion generator as the low-level controller. The TGN infers the next high-level action step at an event-driven inference frequency: a new decision is made only after all currently active robots have completed their ongoing motion segments. This preserves the intended partial-order structure of the task and prevents premature re-planning.

Once the next action step is determined, the GP-based motion generator produces a motion primitive that generalizes the demonstrated trajectory for the corresponding source-target pair. Given arbitrary start and end positions $\mathbf{x}_{\text{new}}^{(\text{start})}$ and $\mathbf{x}_{\text{new}}^{(\text{end})}$, the trained x_{GP} and y_{GP} models predict a canonical trajectory $\mathbf{x}_{\text{GP}}^{(c)}(t')$ for normalized time $t' \in [0, 1]$. This canonical form is then adapted to the new spatial context through inverse scaling, rotation, and translation:

$$\mathbf{x}_{\text{new}}(t') = R^{-1}(\theta_{\text{new}}) \left(\mathbf{x}_{\text{GP}}^{(c)}(t') \cdot \|\mathbf{x}_{\text{new}}^{(\text{end})} - \mathbf{x}_{\text{new}}^{(\text{start})}\| \right) + \mathbf{x}_{\text{new}}^{(\text{start})}, \quad (12)$$

where θ_{new} is the orientation of the target relative to the start, computed as:

$$\theta_{\text{new}} = \arctan 2 \left(y_{\text{new}}^{(\text{end})} - y_{\text{new}}^{(\text{start})}, x_{\text{new}}^{(\text{end})} - x_{\text{new}}^{(\text{start})} \right). \quad (13)$$

This event-driven execution design ensures that robots need not operate in frame-by-frame lockstep. Instead, keyframes are synchronized at completion events: robots may idle while others act, and action labels can change for any subset of robots at each decision point. This naturally supports staggered execution and role switching, as observed in our tasks, while maintaining coherent high-level coordination from few-shot demonstrations.

A limitation of this design is that new decisions are issued jointly only after all active robots complete their current motions. Mid-trajectory replanning for individual robots, necessary for tightly interleaved or highly reactive behaviors is not

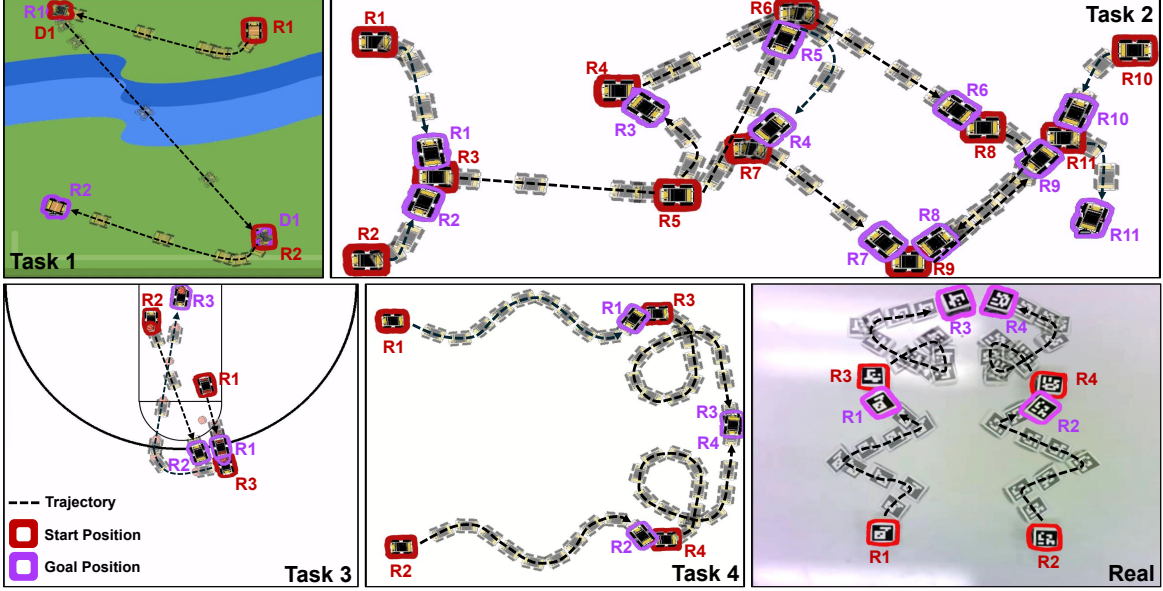


Fig. 3: Visualizations of experimental tasks illustrating diverse multi-robot scenarios: Task 1 features a heterogeneous team of three robots completing a five-step collaborative transport operation; Task 2 evaluates scalability, with eleven robots executing a ten-step coordinated sequence; Task 3 simulates a sports-inspired scenario involving three heterogeneous robots performing a four-step sequence of diverse actions; Task 4 focuses on spatial generalization, requiring four robots to execute complex curved and spiral trajectories in a two-step task; and the Real task reproduces Task 4 in a physical environment to validate both sequence prediction and trajectory generation under realistic conditions.

TABLE I: Summary of Task Properties

Task Description	Multi Sequence	Heterogeneous	Trajectory	Multi Action
Task 1	✓	✓	✗	✓
Task 2	✓	✗	✗	✗
Task 3	✓	✓	✓	✓
Task 4	✓	✗	✓	✗

yet supported. Future work will extend DDACE toward fully asynchronous inference to enable finer-grained coordination in more complex multi-robot tasks.

IV. EXPERIMENTS AND RESULTS

A. Experimental Setup

The performance of the proposed framework was evaluated across four simulated multi-robot tasks, each custom-designed for this study to allow precise control over sequence length, agent heterogeneity, trajectory complexity, and action diversity, enabling targeted evaluation of distinct coordination capabilities under few-shot conditions. As summarized in Table I, the tasks were constructed through an iterative design process in which coordination patterns, role assignments, and movement constraints were explicitly defined to isolate specific aspects of multi-robot learning.

Task 1 evaluates heterogeneous multi-sequence coordination, featuring three robots with different modalities (e.g., UGV and UAV) performing a five-step collaborative transport operation. Task 2 serves as a scalability benchmark, with eleven homogeneous robots executing a ten-step sequence in which dependencies span the entire team; by excluding heterogeneity and complex trajectories, it isolates the challenge of sustaining long-horizon temporal dependencies in large-scale teams. Task 3 assesses heterogeneous multi-action coordination in a sports-inspired setting adapted from a commonly used

basketball ball-screening tactic, where coordinated positioning, passing, and movement outmaneuver a defender. Three heterogeneous robots perform a four-step sequence involving passing, defensive screening, and goal approach, reflecting a widely recognized and generalizable cooperation pattern. Task 4 emphasizes spatial generalization in trajectory learning: in a two-step sequence, four robots execute symmetric curved paths followed by spiral-like trajectories toward their goals, testing the GP model’s ability to reproduce and adapt complex, non-linear paths to new spatial configurations while preserving shape fidelity.

Additional experiments were conducted to assess the influence of task complexity on learning outcomes. In Tasks 2 and 3, the number of robots and the action space per robot were systematically varied. This allowed an analysis of how these variables impact the learning outcomes of the model. Demonstration data were preprocessed and partitioned into training and testing sets, with 90% allocated for training and 10% for evaluation.

Qualitative assessment was performed through simulation of the execution phase, as shown in Fig. 2. Given the initial positions of robots, objects, and goals, the trained sequence predictor provided action assignments for each robot. When movement was required, the corresponding trajectories were generated by the GP model. The sequence was executed iteratively until the task was completed, allowing a comparison between predicted and ground-truth behaviors to assess the model’s ability to capture temporal dependencies and spatial relationships. Quantitative evaluation was performed using two baselines: a conventional GNN with fixed connectivity and a language-model-based method for sequence inference. An ablation study was also included by removing the spectral clustering module and substituting it with a fully connected

TABLE II: Quantitative performance comparison of DDACE against baseline across all experimental tasks.

Methods	Task 1				Task 2				Task 3				Task 4			
	OSR	SSR	GCR	FD	OSR	SSR	GCR	FD	OSR	SSR	GCR	FD	OSR	SSR	GCR	FD
DDACE	1	1	1	0.02	1	1	1	0	1	1	1	0	1	1	1	0.04
DDACE (without spectral clustering)	0	0.2	0.74	0.02	0	0.3	0.59	0	0	0.25	0.50	0	0	0.5	0.74	0.04
GNN	0	0	0.33	0.67	0	0	0.18	1	0	0	0.16	0.93	0	0	0.25	1
LLM (GPT-4o)	1	1	1	-	0	0.3	0.45	-	0	0.25	0.25	-	1	1	1	-

edge structure.

The performance of the proposed model and baseline methods was assessed using metrics, partially adapted from the evaluation framework in [29]. In our framework, the evaluation explicitly distinguishes between temporal sequence prediction and spatial trajectory generation, which are decoupled in DDACE’s architecture:

- Temporal Component – Sequential Action Prediction:
 - *Overall Success Rate (OSR)*: Measures the proportion of tasks in which all robots successfully executed their entire action sequences and satisfied all task-specific goal conditions. This reflects end-to-end temporal coordination quality.
 - *Sequence Success Rate (SSR)*: Measures the percentage of action sequences completed without error, regardless of whether the overall task succeeded. Even when the overall task fails, this metric provides an intuitive measure of how many individual sequences were executed successfully, reflecting per-sequence temporal accuracy.
 - *Goal Condition Recall (GCR)*: Measures the fraction of required goal states achieved by each individual robot, based on its ability to reach designated goal positions or conditions. This captures per-agent temporal accuracy.

- Spatial Component – Trajectory Generation via Gaussian Processes:

- *Fréchet Distance (FD)*: Quantifies the geometric similarity between the GP-generated trajectories and the demonstrated ones, after normalization for scale and position. This directly evaluates spatial path reproduction quality, independent of action sequence correctness.

By grouping OSR, SSR, and GCR under the temporal domain and FD under the spatial domain, the evaluation directly reflects DDACE’s decoupled learning design, enabling independent assessment of sequence prediction reliability and trajectory generation fidelity.

B. Qualitative Analysis

Execution results for all four tasks are visualized in Fig. 3. In Task 1, a heterogeneous transport scenario is depicted, where Robot R1 transfers cargo to Drone D1, which crosses a river and hands it to Robot R2. R2 then completes the delivery to the designated goal. This task involves both wheeled and aerial robots, each operating in a multi-action space including driving, stopping, and cargo transfer. The DDACE framework was observed to perform reliably under such heterogeneous coordination demands.

Task 2 involves a large-scale sequential operation executed by eleven robots. The task begins with R1 and R2 moving

toward R3, followed by R3 proceeding toward R4 via R5. Subsequently, R4 and R5 move toward R6, with R5 halting upon arrival while R4 continues to R7. Independent movements of R6 and R7 to R8 and R9 follow, leading to R8 moving toward R9, then R9 and R10 converging at R11, which finally moves to the goal. This scenario was designed to test scalability, and stable execution was observed over a ten-step sequence.

Task 3 draws inspiration from a ball-screening strategy in basketball. Initially, R2 passes to teammate R3 while opponent R1 approaches for defense. R2 then screens R1, allowing R3 to drive past and proceed toward the goal. This task combines heterogeneous robot roles and a complex multi-action space, including ball passing and dribbling. Accurate trajectory generation was required to ensure R3 moved beyond the screen. The framework effectively captured both the sequential dependencies and trajectory complexity involved.

Task 4 features a simple two-step sequence but emphasizes spatial complexity. Robots R1 and R2 move toward R3 and R4 along symmetric curved paths, after which R3 and R4 navigate spiral-like trajectories to reach the goal. This task was used to assess the model’s ability to learn and reproduce nontrivial path geometries. The results confirmed that DDACE could successfully generalize and replicate such intricate trajectories.

C. Quantitative Analysis

A quantitative evaluation of the proposed framework was performed across all four tasks using the metrics defined in Section IV-A. As shown in Table II, DDACE consistently achieved the highest performance, obtaining perfect scores in OSR, SSR, and GCR across all tasks. Low FD values—ranging from 0.02 in Task 1 to 0.04 in Task 4—indicate that the generated trajectories closely matched those from the demonstrations, demonstrating accurate spatial reproduction and sequence fidelity.

Several baseline comparisons in our study also serve a dual purpose: in addition to providing reference performance, they implicitly act as ablation-like tests for specific DDACE design choices. For example, replacing the refined edge index from the spectral clustering stage with a fully connected graph structure removes the targeted graph refinement step in the temporal module. This configuration—while still functioning as a baseline—revealed significant drops in OSR and SSR, highlighting the importance of identifying critical inter-robot dependencies prior to sequence learning. Without spectral clustering, the absence of structural priors made the learning task more challenging under few-shot conditions, leading to disorganized coordination and lower sequence fidelity. Although GCR remained comparatively higher, it did not consistently result in successful task completion due to disrupted temporal alignment.

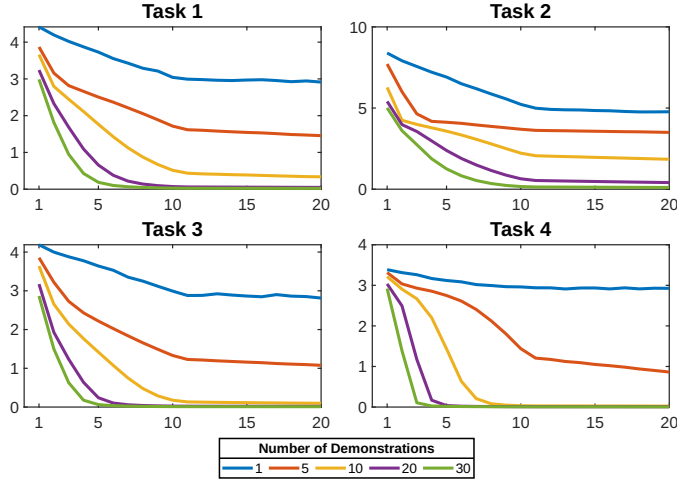


Fig. 4: Training loss versus epoch for Tasks 1–4. Each subplot shows the evolution of the training loss (y-axis) over epochs (x-axis) for different numbers of demonstrations.

Similarly, the end-to-end GNN baseline, which learns both action sequences and trajectories in a single unified model, can also be viewed as a proxy ablation of DDACE’s temporal–spatial decoupling. By removing the explicit separation between sequence prediction and trajectory generation, this configuration demonstrated poor performance—OSR and SSR dropped to zero, GCR values were low, and FD values rose to nearly 1.0. These results underscore both its role as a baseline and the importance of DDACE’s modular design in maintaining coherent multi-robot sequences and high-fidelity trajectories under few-shot constraints.

An additional baseline involved the use of a large language model (LLM) to interpret demonstration data and generate task sequences. The LLM-based approach showed comparable performance to DDACE in Tasks 1 and 4, where sequence structures relied primarily on positional relationships. However, in Task 3—which required reasoning over heterogeneous roles and contextual action coordination—the LLM failed to capture nuanced dependencies, resulting in inaccurate predictions. Similarly, in Task 2, the LLM was unable to generate the complete sequence due to its length, producing only a partial output (up to R6) despite further prompting. These outcomes highlight the current limitations of language-based reasoning in long-horizon and high-complexity multi-robot tasks.

To analyze the effect of demonstration quantity on performance, Fig. 4 presents training loss curves for Tasks 1–4. Across all tasks, additional demonstrations produced faster convergence and lower final loss. In Tasks 1 and 4, where sequence structures are relatively simple, stable convergence was achieved with as few as 10 demonstrations. Task 2, characterized by long-horizon dependencies, required a larger number for reliable learning, though moderate data levels still yielded acceptable results. Task 3, involving heterogeneous roles and multi-action sequences, also showed marked improvements with more demonstrations. These findings indicate that while the model remains effective under severe few-shot constraints, learning efficiency and stability improve with additional data, especially for tasks requiring complex temporal coordination or long-horizon dependencies.

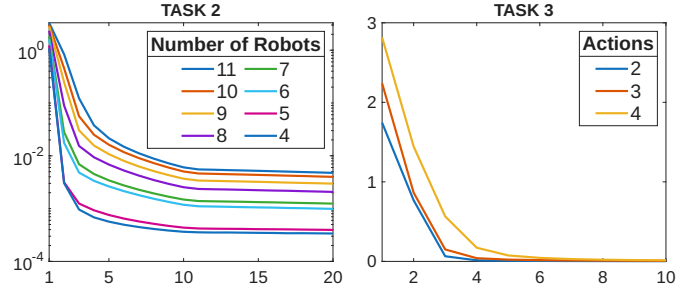


Fig. 5: Training loss analysis across varying robot configurations and action spaces. (Left) Log-scaled training loss versus epoch for different robot team sizes. (Right) Training loss versus epoch for varying action-space complexities.

1) *Case Study 1: Effect of Number of Robots*: This case study focuses on analyzing how a task-level factor—the number of robots—affects learning dynamics, rather than serving as a direct numerical comparison with baselines. Training loss trends for Task 2 under varying robot counts (4 to 11) are depicted in Fig. 5-left, using 30 demonstrations per setting. Loss curves demonstrate that smaller team sizes led to faster convergence and lower final loss due to reduced coordination complexity. In the 4-node case, minimal interdependencies enabled near-zero loss rapidly. Configurations with 6 to 7 nodes preserved the core task structure and maintained efficient learning. In contrast, the 9-11 node scenarios exhibited slower convergence and higher final loss, indicating that increased team size introduced coordination challenges that complicated the learning process. These results emphasize the scalability limits in few-shot settings, where larger team sizes amplify structural complexity and increase learning difficulty, highlighting the type of coordination challenge that DDACE’s temporal–spatial decoupling is designed to mitigate.

2) *Case Study 2: Impact of Action Space Complexity*: Similarly, this case study examines the effect of action space size on convergence behavior, rather than providing a direct baseline comparison. The influence of action space size was examined in Task 3 using three configurations—2, 3, and 4 actions—with 30 demonstrations each (Fig. 5-right). Simpler action spaces (move, stop) enabled rapid and stable convergence. The introduction of a third action (dribble) increased temporal dependencies and slightly delayed convergence. The 4-action setting (including pass) further increased the learning burden, resulting in higher initial loss and slower convergence. These findings indicate that increasing action diversity elevates the reasoning complexity, which in turn slows training, particularly in tasks involving rich inter-agent dependencies or decision-making under temporal constraints. Nonetheless, the model eventually attained low loss in all cases, owing to DDACE’s decoupled framework, which divides key functionalities into separate components, enabling successful learning even under minimal dataset conditions.

D. Real-World Deployment

To evaluate real-world applicability, DDACE was deployed on physical robots to reproduce Task 4 from simulation. This task was chosen because it combines temporal and spatial

learning challenges, with sequential structures and complex trajectories (e.g., curves and spirals), making it well-suited for validating both the sequence predictor and trajectory generator under realistic conditions.

Experiments were conducted on a tabletop setup using Hamster mobile robots [30], compact differential-drive platforms actuated by DC motors and controlled via Bluetooth. An overhead vision system with ArUco markers [31] provided precise visual tracking. The trained models were transferred directly from simulation without fine-tuning, and as shown in Fig. 3 and the supplementary video, the robots reproduced planned behaviors and trajectories with high fidelity, demonstrating DDACE’s few-shot generalization to physical environments.

V. CONCLUSION

This paper presented DDACE, a modular framework designed to tackle the challenge of learning coordinated multi-robot behaviors from limited demonstrations. By decoupling temporal action sequence learning from spatial trajectory generation, DDACE facilitates efficient and scalable policy learning, leveraging graph-based modeling and adaptive trajectory synthesis to capture task dependencies and generalize across varied scenarios. While DDACE assumes optimal demonstrations for few-shot generalization, future work could incorporate retrieval-augmented and semi-supervised few-shot learning [32], [33], broadly framed under meta-learning and data-augmentation, to enhance robustness to imperfect demonstrations. Further directions include improving adaptability to dynamic environments, handling tightly coupled spatiotemporal dependencies, and extending DDACE to real-world datasets such as SportVU [34] for applications in sports analytics and autonomous tactical decision-making.

REFERENCES

- [1] H. Ravichandar, A. S. Polydoros, S. Chernova, and A. Billard, “Recent advances in robot learning from demonstration,” *Annual review of control, robotics, and autonomous systems*, vol. 3, pp. 297–330, 2020.
- [2] B. D. Argall, S. Chernova, M. Veloso, and B. Browning, “A survey of robot learning from demonstration,” *Robotics and autonomous systems*, vol. 57, no. 5, pp. 469–483, 2009.
- [3] A. G. Billard, S. Calinon, and R. Dillmann, “Learning from humans,” *Springer handbook of robotics*, pp. 1995–2014, 2016.
- [4] W. Burgard, M. Moors, C. Stachniss, and F. E. Schneider, “Coordinated multi-robot exploration,” *IEEE Transactions on robotics*, vol. 21, no. 3, pp. 376–386, 2005.
- [5] R. N. Darmanin and M. K. Bugeja, “A review on multi-robot systems categorised by application domain,” in *2017 25th mediterranean conference on control and automation (MED)*. IEEE, 2017, pp. 701–706.
- [6] R. A. Knepper, T. Layton, J. Romanishin, and D. Rus, “Ikeabot: An autonomous multi-robot coordinated furniture assembly system,” in *2013 IEEE International conference on robotics and automation*. IEEE, 2013, pp. 855–862.
- [7] M. V. Balakuntala, U. Kaur, X. Ma, J. Wachs, and R. M. Voyles, “Learning multimodal contact-rich skills from demonstrations without reward engineering,” in *2021 IEEE International Conference on Robotics and Automation (ICRA)*. IEEE, 2021, pp. 4679–4685.
- [8] D. Freelan, D. Wicke, K. Sullivan, and S. Luke, “Towards rapid multi-robot learning from demonstration at the robocup competition,” in *RoboCup 2014: Robot World Cup XVIII 18*. Springer, 2015, pp. 369–382.
- [9] M. A. Simões, R. M. da Silva, and T. Nogueira, “A dataset schema for cooperative learning from demonstration in multi-robot systems,” *Journal of Intelligent & Robotic Systems*, vol. 99, no. 3, pp. 589–608, 2020.
- [10] S. S. Kannan, V. L. Venkatesh, R. K. Senthilkumaran, and B.-C. Min, “Uppled: Uav path planning for inspection through demonstration,” in *2023 IEEE/RSJ International Conference on Intelligent Robots and Systems (IROS)*. IEEE, 2023, pp. 1126–1133.
- [11] M. F. Martins and Y. Demiris, “Learning multirobot joint action plans from simultaneous task execution demonstrations.” in *AAMAS*, 2010, pp. 931–938.
- [12] K. Sullivan and S. Luke, “Hierarchical multi-robot learning from demonstration,” in *Proceedings of the Robotics: Science and Systems Conference*, 2011.
- [13] D. Freelan, D. Wicke, K. Sullivan, and S. Luke, “Towards rapid multi-robot learning from demonstration at the robocup competition,” in *Robot Soccer World Cup*. Springer, 2014, pp. 369–382.
- [14] S. Chernova and M. Veloso, “Interactive policy learning through confidence-based autonomy,” *Journal of Artificial Intelligence Research*, vol. 34, pp. 1–25, 2009.
- [15] B. Huang, M. Ye, S.-L. Lee, and G.-Z. Yang, “A vision-guided multi-robot cooperation framework for learning-by-demonstration and task reproduction,” in *2017 IEEE/RSJ International Conference on Intelligent Robots and Systems (IROS)*. IEEE, 2017, pp. 4797–4804.
- [16] L. Brunke, M. Greeff, A. W. Hall, Z. Yuan, S. Zhou, J. Panerati, and A. P. Schoellig, “Safe learning in robotics: From learning-based control to safe reinforcement learning,” *Annual Review of Control, Robotics, and Autonomous Systems*, vol. 5, pp. 411–444, 2022.
- [17] V. L. Venkatesh and B.-C. Min, “Learning from demonstration framework for multi-robot systems using interaction keypoints and soft actor-critic methods,” in *2024 IEEE/RSJ International Conference on Intelligent Robots and Systems (IROS)*. IEEE, 2024, pp. 10 754–10 761.
- [18] J. Blumenkamp, S. Morad, J. Gielis, Q. Li, and A. Prorok, “A framework for real-world multi-robot systems running decentralized gnn-based policies,” in *2022 International Conference on Robotics and Automation (ICRA)*. IEEE, 2022, pp. 8772–8778.
- [19] B. Chandrasekaran, “A survey of path planning and navigation in multi-robotic systems,” in *2023 1st International Conference on Advanced Engineering and Technologies (ICONNIC)*. IEEE, 2023, pp. 38–42.
- [20] Q. Li, F. Gama, A. Ribeiro, and A. Prorok, “Graph neural networks for decentralized multi-robot path planning,” in *2020 IEEE/RSJ international conference on intelligent robots and systems (IROS)*. IEEE, 2020, pp. 11 785–11 792.
- [21] Z. Wu, Z. Li, D. Zhu, Q. Liao, and W. Yao, “A multi-robot task allocation method based on graph attention network and unsupervised learning,” in *2024 IEEE International Conference on Unmanned Systems (ICUS)*. IEEE, 2024, pp. 1222–1227.
- [22] M. Goarin and G. Loianno, “Graph neural network for decentralized multi-robot goal assignment,” *IEEE Robotics and Automation Letters*, 2024.
- [23] Z. Chekakta, N. Aouf, S. Govindaraj, F. Polisano, and G. De Cubber, “Towards learning-based distributed task allocation approach for multi-robot system,” in *2024 10th International Conference on Automation, Robotics and Applications (ICARA)*. IEEE, 2024, pp. 34–39.
- [24] H. Zhang, J. Cheng, L. Zhang, Y. Li, and W. Zhang, “H2gnn: Hierarchical-hops graph neural networks for multi-robot exploration in unknown environments,” *IEEE Robotics and Automation Letters*, vol. 7, no. 2, pp. 3435–3442, 2022.
- [25] S. Chen, Y. Cao, Y. Kang, J. Di, B. Sun, and X. Wang, “Spatiotemporal graph policy gradients for multi-robot formation control,” in *2021 7th International Conference on Big Data and Information Analytics (BigDIA)*. IEEE, 2021, pp. 436–439.
- [26] A. Goeckner, Y. Sui, N. Martinet, X. Li, and Q. Zhu, “Graph neural network-based multi-agent reinforcement learning for resilient distributed coordination of multi-robot systems,” in *2024 IEEE/RSJ International Conference on Intelligent Robots and Systems (IROS)*. IEEE, 2024, pp. 5732–5739.
- [27] Z. Zhu, M. Liu, L. Mao, B. Kang, M. Xu, Y. Yu, S. Ermon, and W. Zhang, “Madiff: Offline multi-agent learning with diffusion models,” *Advances in Neural Information Processing Systems*, vol. 37, pp. 4177–4206, 2024.
- [28] L. Meng, M. Wen, C. Le, X. Li, D. Xing, W. Zhang, Y. Wen, H. Zhang, J. Wang, Y. Yang *et al.*, “Offline pre-trained multi-agent decision transformer,” *Machine Intelligence Research*, vol. 20, no. 2, pp. 233–248, 2023.
- [29] S. S. Kannan, V. L. Venkatesh, and B.-C. Min, “Smart-llm: Smart multi-agent robot task planning using large language models,” in *2024 IEEE/RSJ International Conference on Intelligent Robots and Systems (IROS)*. IEEE, 2024, pp. 12 140–12 147.

- [30] A. Lee, W. Jo, S. S. Kannan, and B.-C. Min, “Investigating the effect of deictic movements of a multi-robot,” *International Journal of Human-Computer Interaction*, vol. 37, no. 3, pp. 197–210, 2021.
- [31] S. Garrido-Jurado, R. Muñoz-Salinas, F. Madrid-Cuevas, and M. Marín-Jiménez, “Automatic generation and detection of highly reliable fiducial markers under occlusion,” *Pattern Recognition*, vol. 47, no. 6, pp. 2280–2292, 2014.
- [32] M. Du, S. Nair, D. Sadigh, and C. Finn, “Behavior Retrieval: Few-Shot Imitation Learning by Querying Unlabeled Datasets,” in *Proceedings of Robotics: Science and Systems*, Daegu, Republic of Korea, July 2023.
- [33] P. Wu, K. Hakhamaneshi, Y. Du, I. Mordatch, A. Rajeswaran, and P. Abbeel, “Semi-supervised one shot imitation learning,” *Reinforcement Learning Journal*, vol. 5, pp. 2284–2297, 2025.
- [34] K. Linou, D. Linou, and M. d. Boer, “NBA-Player-Movements,” 9 2016. [Online]. Available: <https://github.com/linouk23/NBA-Player-Movements>